Environmental Science and Pollution Research (2018) 25:34247–34261
https://doi.org/10.1007/s11356-018-3322-2

RESEARCH ARTICLE

Silver and gold nanoparticles biosynthesized by aqueous extract of burdock root, *Arctium lappa* as antimicrobial agent and catalyst for degradation of pollutants

Thi Thanh-Ngan Nguyen[1,2] · Thanh-Truc Vo[2,3] · Bich Ngoc-Huong Nguyen[4] · Dinh-Truong Nguyen[4] · Van-Su Dang[5] · Chi-Hien Dang[2,3] · Thanh-Danh Nguyen[1,2]

Received: 13 May 2018 / Accepted: 24 September 2018 / Published online: 6 October 2018

Abstract

This study presents an efficient and facile method for biosynthesis of silver nanoparticles (AgNPs) and gold nanoparticles (AuNPs) using aqueous extract of burdock root (BR), *A. lappa*, and their applications. The nanoparticles were characterized by ultraviolet-visible spectrophotometry, X-ray diffraction, transmission electron microscopy, energy dispersive X-ray, thermogravimetry, and differential thermal analysis. AgNPs capped the BR extract (BR-AgNPs) possessed roughly spherical geometry with an average diameter of 21.3 nm while uneven geometry of AuNPs capped the BR extract (BR-AuNPs) showed multi shapes in average size of 24.7 nm. The BR-AgNPs strongly inhibited five tested microorganism strains. In particular, the nanoparticles showed excellent catalytic activity for the conversion of pollutants within wastewater. Pseudo-first-order rate constants for the degradation of 4-nitrophenol, methyl orange, and rhodamine B were respectively found 6.77×10^{-3}, 3.70×10^{-3}, and 6.07×10^{-3} s^{-1} for BR-AgNPs and 6.87×10^{-3}, 6.07×10^{-3}, and 7.07×10^{-3} s^{-1} for BR-AuNPs.

Keywords Nanoparticles · Degradation · Pollutants · *Arctium lappa* · Antimicrobial · Catalyst

Introduction

Nanomaterials are particularly considered in recent decades due to distinctive properties in contrast to the bulk form. Among nanomaterials, metallic nanoparticles (MNPs) played a crucial role in various fields such as biomedicine, electronics, energy science, agriculture, textile, environment, and drug delivery system (Albanese et al. 2012; Misha et al. 2014; Pramanik et al. 2015; Tareq et al. 2017; Mahadevan et al. 2017; Zhao et al. 2016; Naraginti and Li 2017; Fayaz et al. 2010). Although synthesis of MNPs using chemicals was successful in generating pure and well-defined nanoparticles, it is quite expensive and causes dangers to the life environment (Bello et al. 2017; Hernandez-Pinero et al. 2016). Thus, it is necessary to explore green approaches for the MNPs synthesis which provides additional advantages for the applicability of nanoparticles in biomaterials as well as industrial products.

The biosynthesized MNPs using friendly environmental and economic resources is the current trend due to cost-efficiency, eco-friendly operation, and easy synthesis at large scales (Sathishkumar et al. 2009; Singh et al. 2015; Khan et al. 2015; Morales-Luckie et al. 2016; Iravani 2011; Ahmed et al. 2016). The properties of the biosynthesized MNPs may differ from materials prepared by other methods. The biosynthesized MNPs can enhance stability and biocompatibility and reduce toxicity, mainly due to coating them with biogenic surfactants or capping agents (Pramanik et al. 2014; Zhang et al. 2016; Rafique et al. 2017). There are various

Responsible editor: Philippe Garrigues

✉ Thanh-Danh Nguyen
danh5463bd@yahoo.com

[1] Institute of Research and Development, Duy Tan University, Da Nang City, Vietnam

[2] Institute of Chemical Technology, Vietnam Academy of Science and Technology, 1 Mac Dinh Chi Street, District 1, Ho Chi Minh City, Vietnam

[3] Graduate University of Science and Technology, Vietnam Academy of Science and Technology, 18 Hoang Quoc Viet, Cau Giay, Hanoi, Vietnam

[4] School of Biotechnology, Tan Tao University, Long An Province, Vietnam

[5] Department of Chemical Technology, Ho Chi Minh City University of Food Industry, Ho Chi Minh, Vietnam

natural resources such as plant extracts, microorganisms, algae, fungi, and enzymes that possess both specially stabilized and reductive properties (Singh et al. 2016a, 2016b; Iravani 2011). Particularly, the plant extracts were widely used as popular biosynthetic sources because they contained many organic-reducing agents such as phenolic acid, flavonoids, alkaloids, and terpenoids which were mainly responsible for the redox reactions in the biosynthesis of MNPs (Bello et al. 2017; Arya et al. 2017).

Due to efficient separation and recycling in comparison with the traditional catalysts, MNPs are also particularly considered for catalyst of organic reactions (Nguyen et al. 2018a). MNPs possessing high surface to volume ratio, thus providing many highly active metal uncoordinated sites, were widely used within catalytic treatment of wastewater and reduction of environmental contaminants such as nitro aromatic compounds and polluting dyes (Schrofel et al. 2014; Nguyen et al. 2018b). Few previous reports revealed that AgNPs and AuNPs might catalyze effectively for the degradation of these pollutants in aqueous medium. In general, the biosynthesized MNPs showed better catalytic efficiency than chemically synthesized materials. It should be noted that the catalytic performance of MNPs significantly depends on the molecules capping the biosynthesized nanomaterials (Nag et al. 2018).

In this article, we report biosynthesis of AgNPs and AuNPs by aqueous extract of burdock root, *Arctium lappa*. The effect of reaction parameters such as initial metallic ion concentration, ratios of the extract volume to salt solution volume, and incubation time on efficiency of MNPs synthesis was investigated. The biosynthesized MNPs were evaluated antimicrobial activity and catalytic activity for degradation of pollutants in aqueous medium including 4-nitrophenol, methyl orange, and rhodamine B.

Experimental

Materials

All chemicals and reagents for the synthesis were analytical grade and used as received without further purification. Hydrogen tetrachloroaurate (III) hydrate ($HAuCl_4 \cdot 3H_2O$), Silver nitrate ($AgNO_3$), 4-nitrophenol (4-NP), Methyl orange (MO), Rhodamine B (RhB), and Sodium tetrahydridoborate ($NaBH_4$) were purchased from Acros (Begium). Burdock root, *Arctium lappa* Linne, was provided by Khai Minh Macrobiotics (Ho Chi Minh City). Distilled water was used throughout.

Plant extract preparation

The dry burdock roots were finely grinded up powder by using an electronic blender. The burdock root powder (10 g) was boiled with distilled water (100 mL) for 1 h. The obtained mixture was filtered under reduced pressure condition with Whatman filter paper No.1 and stored in the refrigerator at 4–10 °C for further experiments.

Biosynthesis of silver and gold nanoparticles

The burdock root extract was added into the solution of $AgNO_3$ or $HAuCl_4 \cdot 3H_2O$ under continuous stirring and dark condition at 1200 rpm and 90 °C. The formation of the AgNPs and AuNPs was visually observed by changing in the color of the reaction mixtures and scanning the UV-Vis spectra from 200 to 800-nm range using a UV-Vis spectrophotometer (JASCO V-630 spectrophotometer, USA). After completing reduction, the BR-AgNPs and BR-AuNPs were collected by centrifugation at 10,000 rpm for 10 min and washed thrice with distilled water to remove unconverted metal ions or the impurities. Finally, the dried powder of BR-AgNPs and BR-AuNPs was obtained after drying in an oven at 90 °C overnight and stored to use for further investigation.

Optimization of reaction parameters

The biosynthesis reaction of AgNPs and AuNPs is very sensitive and depends on certain important parameters, e.g., time of reaction, concentration of metallic ion, volume rate of plant extract to metallic ions, and the temperature of reaction (Albanese et al. 2012). In this study, the MNPs production was optimized with three following parameters to find out the best condition for the synthesis of nanoparticles.

In order to optimize metallic salt concentrations, reactions were carried out by varying concentrations of the salts, $AgNO_3$ and $HAuCl_4 \cdot 3H_2O$, i.e., 0.5 mM, 1.0 mM, 1.5 mM, and 2.0 mM with volume rate of metal salts to plant extract (20:1) under the same stirring speed (1200 rpm) and temperature (90 °C) for 2 h. Reduction was monitored by UV-vis measurements.

For the effect of plant extract rate, synthesis of MNPs was optimized with different ratios of salt solution volume to the extract volume, i.e., 2:1, 5:1, 10:1, 20:1, and 30:1 under constant salt concentration (1 mM), reaction time (2 h), stirring speed (1200 rpm), and temperature (90 °C).

Finally, the reaction mixtures were monitored at regular time interval from 0 to 180 min with concentration of metallic ions (1 mM) and volume rate of metal salt to plant extract (20:1) under stirring speed (1200 rpm) and temperature of reaction (90 °C) for 2 h.

Characterization of AgNPs and AuNPs

X-ray diffraction analysis (XRD)

X-ray diffraction analysis (XRD) performed the crystalline nature of the nanoparticles on X-ray diffractometer

BRUKER, Model-D8 ADVANCE, Germany, which operated the nanoparticles in powder form under the following conditions: voltage 40 kV, current 40 mA with CuKα radiation of 1.5406 nm wavelength at a scanning rate 0.1°/s, step size 0.03θ over the 2θ range from 20° to 80°.

Transmission electron microscope (TEM) and high-resolution transmission electron microscope (HRTEM) measurement

The morphology and size distribution of biosynthesized BR-AgNPs and BR-AuNPs were evaluated by using TEM images that were taken by JEOL JEM-1400 TEM set at 120 kV of accelerating voltage. The crystal structure analysis of atoms was done on HRTEM, Fecnai G2 20 S-TWIN, FEI set at 200 kV. A drop of AgNPs and AuNPs solutions was used for TEM and HRTEM analysis.

Fourier-transform infrared radiation (FTIR)

To investigate the possible functional group present as a reducing, stabilizing, and capping agent on surface of synthesized nanoparticles, the biosynthesized BR-AgNPs and BR-AuNPs and the plant extract were analyzed by Fourier-transform infrared (FTIR) measurement. The FTIR spectra were recorded on a Bruker, Tensor 27 FTIR spectrophotometer (Germany) with the wavelength ranging from 500 to 4000 cm^{-1}.

Energy dispersive X-ray spectroscopy (EDX)

An energy dispersive X-ray spectroscopy (EDX) analyzer Horiba, EMAX ENERGY EX-400 was used to analyze elements in micro-area and the condition of elements distribution of the AgNPs and AuNPs products. The nanoparticles powder samples were used for EDX measurement.

Thermogravimetry (TG) and different thermal analysis (DTA)

To determine the thermal behaviors of the nanoparticles, a LabSys evo S60/58988 Thermoanalyzer (Setaram, France) was used for simultaneous thermal analysis combining thermogravimetry (TG) analysis and different thermal analysis (DTA). The oven-dried powder samples of AgNPs and AuNPs were heated from room temperature to 800 °C with a heating rate of 10 °C/min in the air atmosphere.

Antimicrobial activity of silver and gold nanoparticles

The disk diffusion method [Hadacek and Greger 2000] was used to measure the antimicrobial activity of the biosynthesized BR-AgNPs and BR-AuNPs against two Gram-negative bacteria strains (*Escherichia coli*, *Agrobacterium tumefaciens*) and two Gram-positive bacterium strains (*Lactobacillus acidophilus*, *Staphylococcus aureus*) as well as for a fungus strain (*Trichoderma harzianum*). Microorganisms were procured originally from School of Biotechnology, Tan Tao University, Vietnam. Briefly, 20 μL of each aliquot was applied to 9-mm-diameter paper disks, and all paper disks were placed on the agar plates previously spread with 1-mL bacterial culture (10^6 CFU/mL). The samples were prepared by dissolving the AgNPs and AuNPs solutions to the required mass i.e., 0.1 μg, 0.2 μg, 0.3 μg, 0.5 μg, 1.0 μg, 2.0 μg, 3.0 μg, and 4.0 μg. The standard antibiotic ampicillin (0.01 mg/mL) was used as positive control, and Luria Bertani broth for antibacterial test and potato dextrose broth for antifungal test were used as negative controls. The inoculated disks were incubated at 37 °C/12 h for the bacteria and 28 °C/36 h for the fungus. Antimicrobial activity was determined by measuring the diameters of inhibition zone formed around the paper disks in millimeters (Balouiri et al. 2016).

Catalytic activity of silver and gold nanoparticles

The catalytic activity of AgNPs and AuNPs was evaluated by the reduction of the pollutants including 4-NP, MO, and RhB with excess amount of $NaBH_4$. An aqueous solution of the pollutants (0.1 mM) and $NaBH_4$ (1.0 M) was prepared with distilled water. To initiate catalytic reduction process, the mixtures of 2.5 mL of the pollutants (0.1 mM) and 0.5 mL of $NaBH_4$ (1 M) were added into the cuvette. Then, 1 mg of the obtained nanoparticles was added into the reaction mixture. The reduction of the pollutants was monitored at regular time interval by UV-vis spectrophotometer at the range between 200 and 800-nm wavelengths. The addition of 1 mg of MNPs led to a rapid decrease in the intensity of the absorption peaks of 4-NP, MO, and RhB at wavelengths 400, 464, and 554 nm, respectively.

Results and discussion

Biosynthesis of silver and gold nanoparticles

The plant has been shown to be a great source of bioactive compounds which can be used for environmentally friendly synthesis of MNPs. In the present work, route of AgNPs and AuNPs biosynthesis using aqueous extract of dried burdock root (BR), *Arctium lappa*, are illustrated in Fig. 1. A solution colored yellow was obtained after the dried BR samples were refluxed for 2 h and completed filtered process. Reaction condition for MNPs biosynthesis using the extract was optimized with heating at 90 °C. The formation of MNPs might be confirmed by colored change recognition and UV-Vis measurement (Fig. 2). In the UV-vis spectra, the BR extract absorbed λ_{max} values at 296 and 326 nm, assigned respectively to $n \rightarrow \pi^*$ and $n \rightarrow n^*$

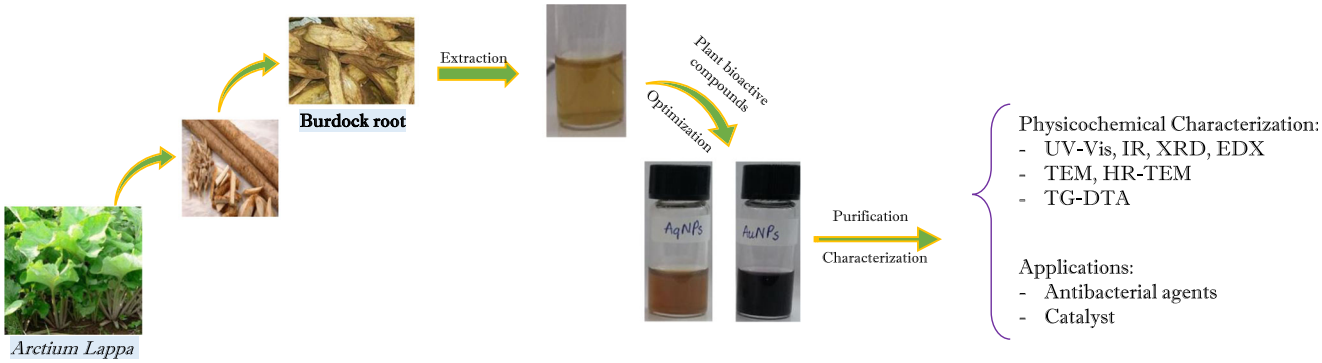

Fig. 1 Schematic illustration of biosynthesis of BR-AgNPs and BR-AuNPs from *A. lappa* extract and their characterizations and applications

transitions of plant aromatic compounds while the characterized surface plasmon resonance (SPR) band of AgNPs and AuNPs solutions was observed at 435 and 540 nm, respectively. In the next step, the optimization of stable nanoparticle formation was carried out by UV-vis spectroscopy measurement. Further, the biosynthesized nanoparticles were purified and characterized by physicochemical analytical techniques and applied for antibacterial and catalytic activities.

Optimization of reaction parameters

It is well known that shape and size of MNPs depend on different reaction conditions. The change of the MNPs might be recorded by SPR absorption bands. Thus, optimization of the production condition based on the UV-vis absorption spectra can be easily carried out to gain important insight of the reduction of the metallic ions to the nanoparticles. In the present work, the principle parameters involved in the optimization process were (1) salt concentrations, (2) ratios of salt solution volume to the extract volume, and (3) reaction time.

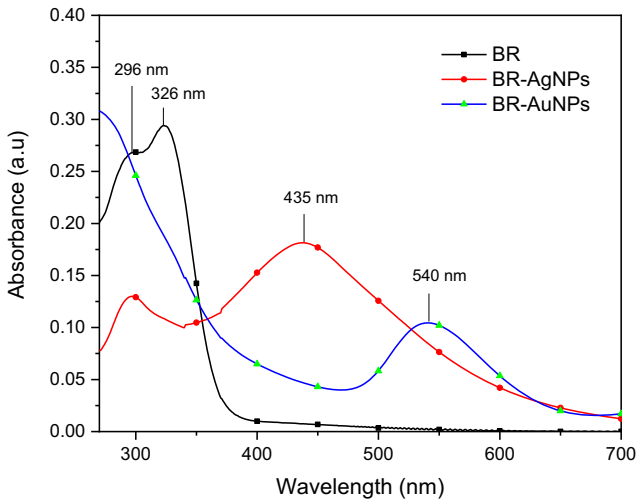

Fig. 2 UV-Vis spectroscopy of BR extract, BR-AgNPs, and BR-AgNPs solutions

The optimization of BR-AgNPs biosynthesis was presented in Fig. 3. The results showed that the effect of different concentrations of Ag^+ ions in the reaction mixture on absorbance of the SPR band was as a function of the salt concentration (Fig. 3a). When the Ag^+ solutions were concentrated around 0.5–2.0 mM, increasing maximum density of the SPR bands was observed. Furthermore, no clear peak of SPR band was found with the diluted Ag^+ solution at 0.5 mM while a significant red shift with the high concentrations was observed, attributed to change of the sizes and shapes of the nanoparticles formed.

The ratios of Ag^+ solution volume to BR extract volume were investigated in a range from 2:1 to 30:1 (Fig. 3b). The results showed that the absorbance of the SPR band grows with the increase of these ratios. Intensive SPR peaks around 435 nm were not observed at the rates less than 10:1 while slight red shifts of λ_{max} values were found at the higher rates.

To study the effect of time on the synthesis of the nanoparticles, the reaction was monitored for each regular time interval of 30 min (Fig. 3c). The results showed that the SPR band was unambiguously apparent within initial 30 min, and the absorbance of the band increased with the reaction time. The reaction was almost completed for 120 min. Moreover, a significant variation in λ_{max} values was observed that a red shift was found from 407 nm to 426 nm when the reaction time was increased from 30 min to 120 min. This should be related to change of the size of the biosynthesized nanoparticles.

Regarding the synthesis of AuNPs based on similar study of AgNPs, the synthesis with varied gold ion concentrations slightly differed from the results of AgNPs synthesis (Fig. 4a). The SPR band at 540 nm was clearly observed in UV-vis spectra of all tested concentrations even the diluted concentration (0.5 mM) and the absorbance increased according to the concentration of Au^{3+} ion. Additionally, the effect of varied concentration on change of λ_{max} values was not so significant.

The increased absorbance of the SPR band was observed when the rates of Au^{3+} solution volume to the BR extract volume were increased (Fig. 4b), and there were no produced AuNPs when the rates used were below 10:1. In addition,

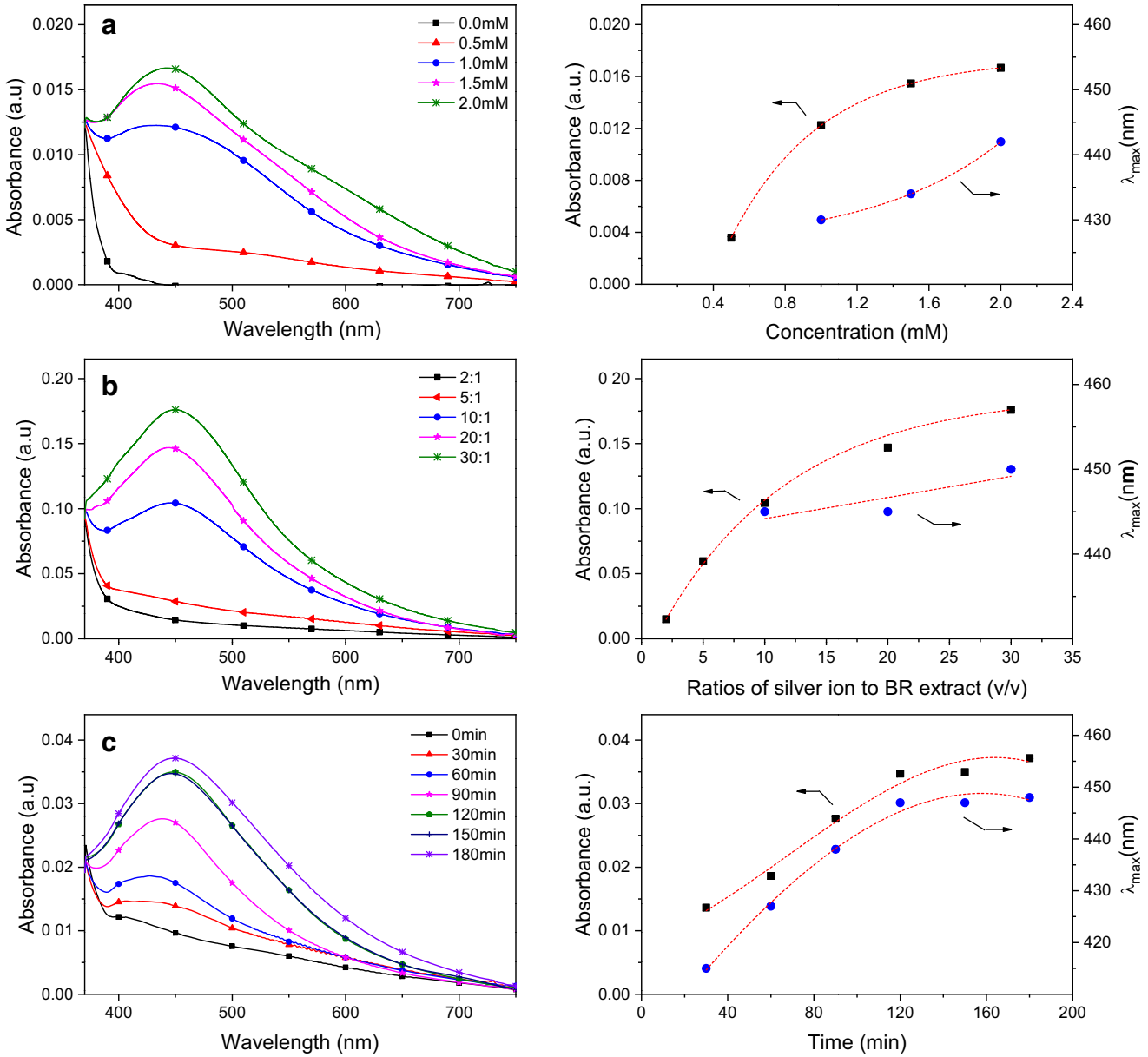

Fig. 3 UV-vis spectra (left) and plots of parameters versus absorbance and λ_{max} values (right): concentrations of Ag^+ solution (**a**), ratios of Ag^+ solution volume (1 mM) to the extract volume (**b**), and reaction time (**c**)

λ_{max} values were affected by these rates which showed no change of size and shape of BR-AuNPs.

For study of reaction time, the reduction of gold ions seems more rapid in comparison with AgNPs formation (Fig. 4c). The results showed that the conversion achieved over 50% in initial 30 min, and a slightly red shift of λ_{max} values along with reaction time was also observed.

Based on the optimization process, the samples for further studies on characterization and application of both MNPs were prepared at metallic ion concentration of 2.0 mM, the ratios of 30:1 and stirred for 120 min at 90 °C.

FTIR spectroscopy

The infrared absorption measurements were carried out in order to identify the presence of various functional groups in the BR extract and biosynthesized MNPs as shown in Fig. 5. All samples showed similar absorption bands. It is a fact that MNPs might be capped and stabilized by biomolecules of BR extract. The phytochemical analysis of BR extract reveals the presence of polyphenol, steroids, terpenoids, glucides, and proteins (Chan et al. 2011; Tousch et al. 2014). In BR extract, the bands were observed at 596, 818, 1033, 1246, 1336, 1430,

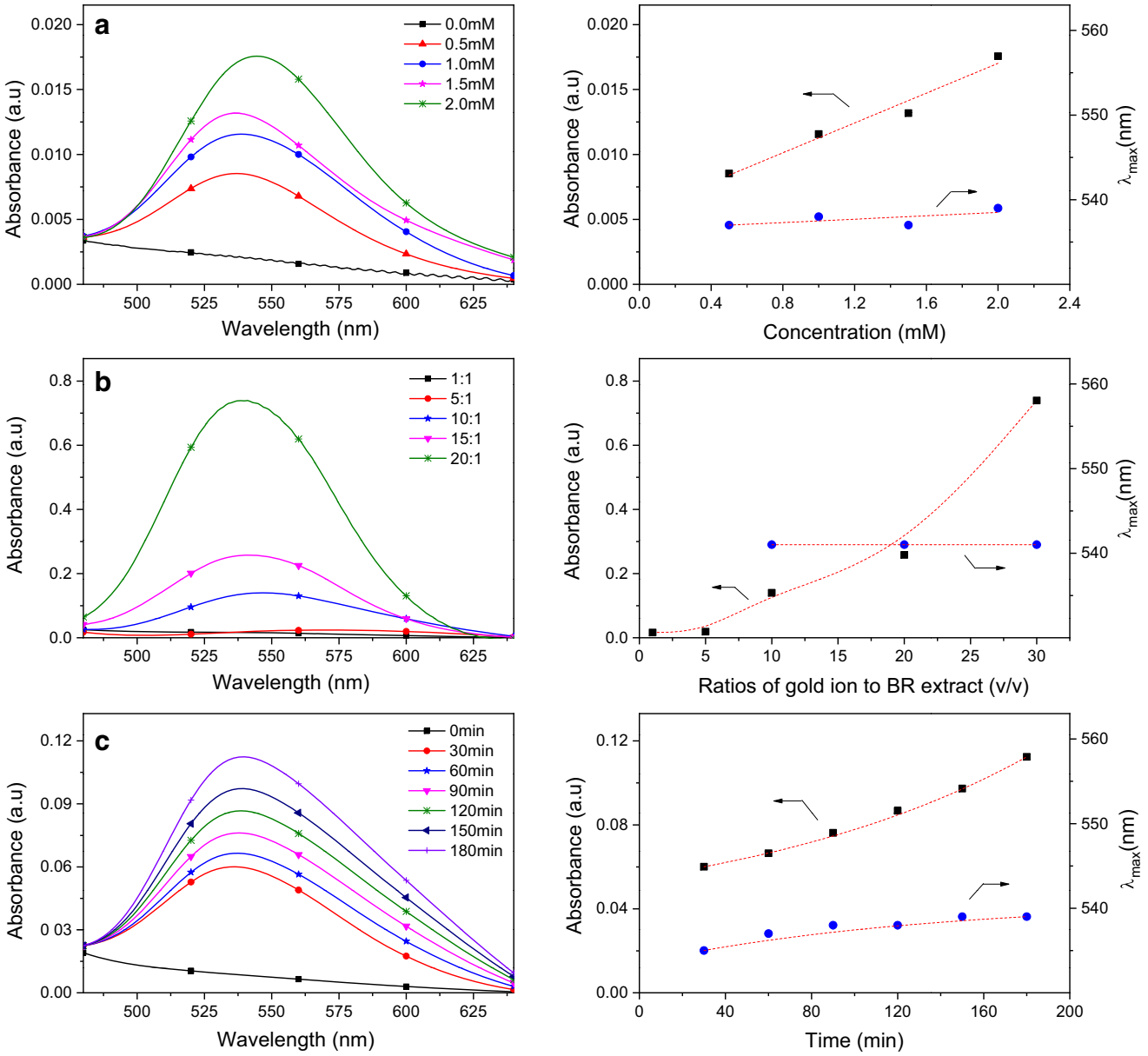

Fig. 4 UV-vis spectra (left) and plots of parameters versus absorbance and λ_{max} values (right): concentrations of Au^{3+} solution (**a**), ratios of Au^{3+} solution volume (1 mM) to the extract volume (**b**), and reaction time (**c**)

1633, 2870, 2932, and 3375 cm^{-1}. After the reduction, the spectra of MNPs were shifted to new positions such as BR-AgNPs bands at 632, 1036, 1384, 1624, 2853, 2923, and 3421 cm^{-1} and BR-AuNPs bands at 660, 1034, 1401, 1627, 2854, 2923, and 3431 cm^{-1}. The spectra showed the bands at around 3400 cm^{-1} ascribed to O–H stretching vibration indicating the presence of glucides and polyphenol. Bands at 2930 and 2850 cm^{-1} region correspond to C–H stretching of aromatic compounds. The strong intense bands at 1390 cm^{-1} and 1040 cm^{-1} were respectively assigned to N–H and C–N stretch vibrations of proteins in the BR extract. These functional groups might play an important role in stabilization and capping of metallic nanoparticles (Prakash et al. 2013). The bands at around 600 cm^{-1} could be attributed to C–Cl stretching in characteristic of alkyl halides.

X-ray diffraction (XRD)

The crystalline nature of the biosynthesized nanoparticles was confirmed by X-ray crystallography. Figure 6 describes the XRD diffractogram of the biosynthesized MNPs. The XRD pattern showed peaks at 2θ values of 38.12, 44.33, 64.49, and 77.54 for AgNPs; and 38.08, 44.42, 64.52, and 77.81 for AuNPs which respectively corresponds to crystal planes (111), (200), (220), and (311) of the face-centered cubic structure. XRD analysis reveals the preferential orientation of the

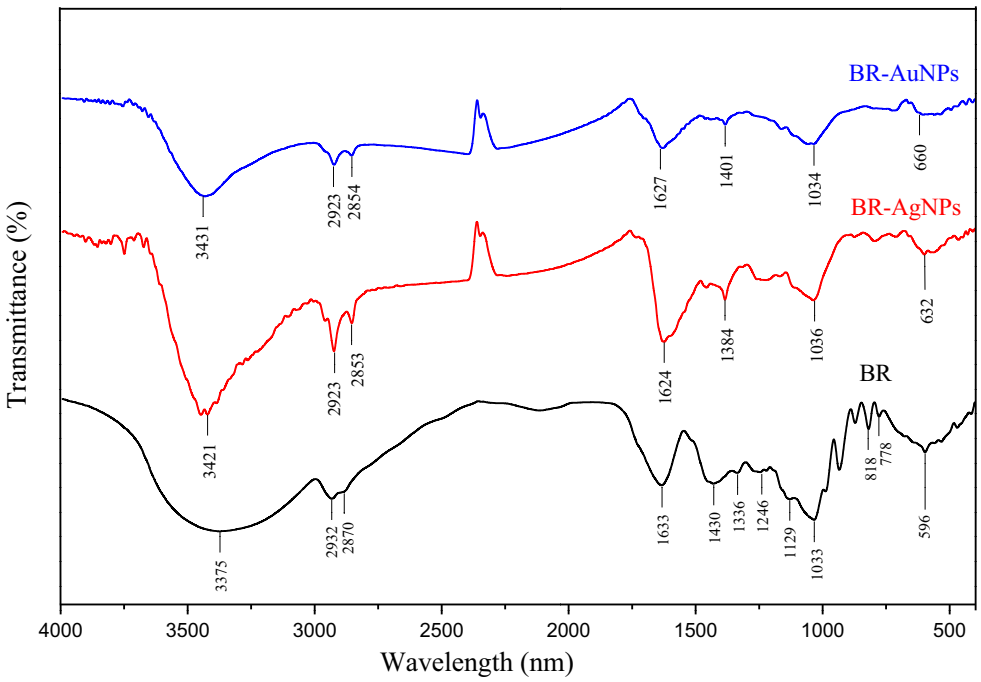

Fig. 5 FTIR spectra of BR extract, BR-AgNPs, and BR-AuNPs

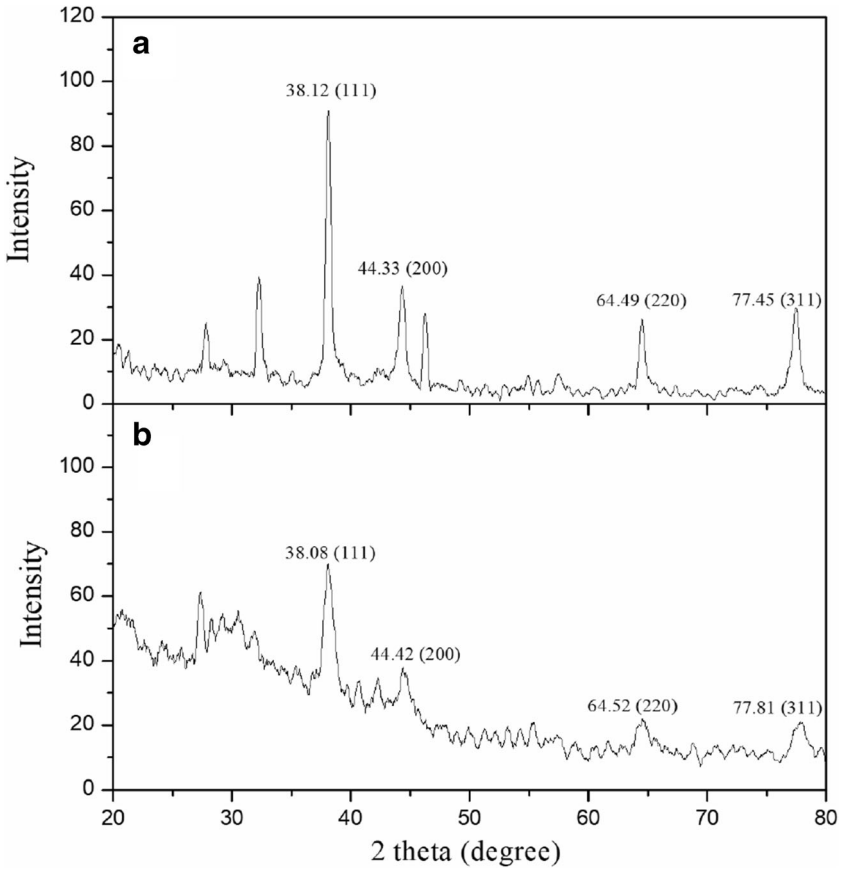

Fig. 6 XRD pattern of synthesized BR-AgNPs (**a**) and BR-AuNPs (**b**)

crystals towards (111) plane with the strong intensity of the diffraction peaks in both MNPs.

Energy dispersive X-ray (EDX) and transmission electron microscope (TEM) analysis

Size, shape, and surface morphology of the MNPs were observed by TEM and HRTEM images. TEM images and particle size distribution (Figs. 7a, b and 8a, b) showed that AgNPs had roughly spherical geometry with an average diameter of 21.3 nm while uneven geometry of AuNPs with multi shapes such as spherical, triangular, and hexagonal shapes was observed in average size of 24.7 nm. Difference in shape and size of MNPs can be due to low reduction potential of AuNPs compared to AgNPs and the difference in phytochemicals of BR extract, which stabilizes AgNPs and AuNPs (Sheny et al. 2011; Joseph and Mathew 2015a; Francis et al. 2017). Crystal lattice of the MNPs is clearly apparent in HRTEM images (Figs. 7c and 8c). The fringe lattice of the AgNPs and AuNPs corresponding to the (111) plane has a spacing of 0.24 nm and 0.22 nm, respectively (Joseph and Mathew 2015a; Dutta et al. 2017).

The elemental composition of BR-AgNP and BR-AuNP was characterized using EDX spectroscopy. It is a plot of ionization energy (keV) versus intensity of X-rays (counts). The BR-AgNP spectrum (Fig. 7d) appeared a strong signal at 2.95 keV originated from elemental silver while BR-AuNP gave three signals of elemental gold at 2.11, 8.46, and 9.72 keV (Fig. 8d) (Dutte et al., 2017). Additionally, the signals relating to elemental carbon (0.01 keV) and oxygen (0.27 keV) in both spectra indicated phytochemicals in the BR extract coated on the MNPs. From EDX spectra data, average contents of silver in BR-AgNPs and gold in BR-AuNPs were found to be as high as 86.3% (*w*/*w*) and 83.1% (*w*/*w*), respectively.

Thermal behaviors

In order to identify the role of BR extract as capping agent, TG-DTA curves of BR extract, BR-AgNPs, and BR-AuNPs in the air atmosphere are simultaneously measured up to

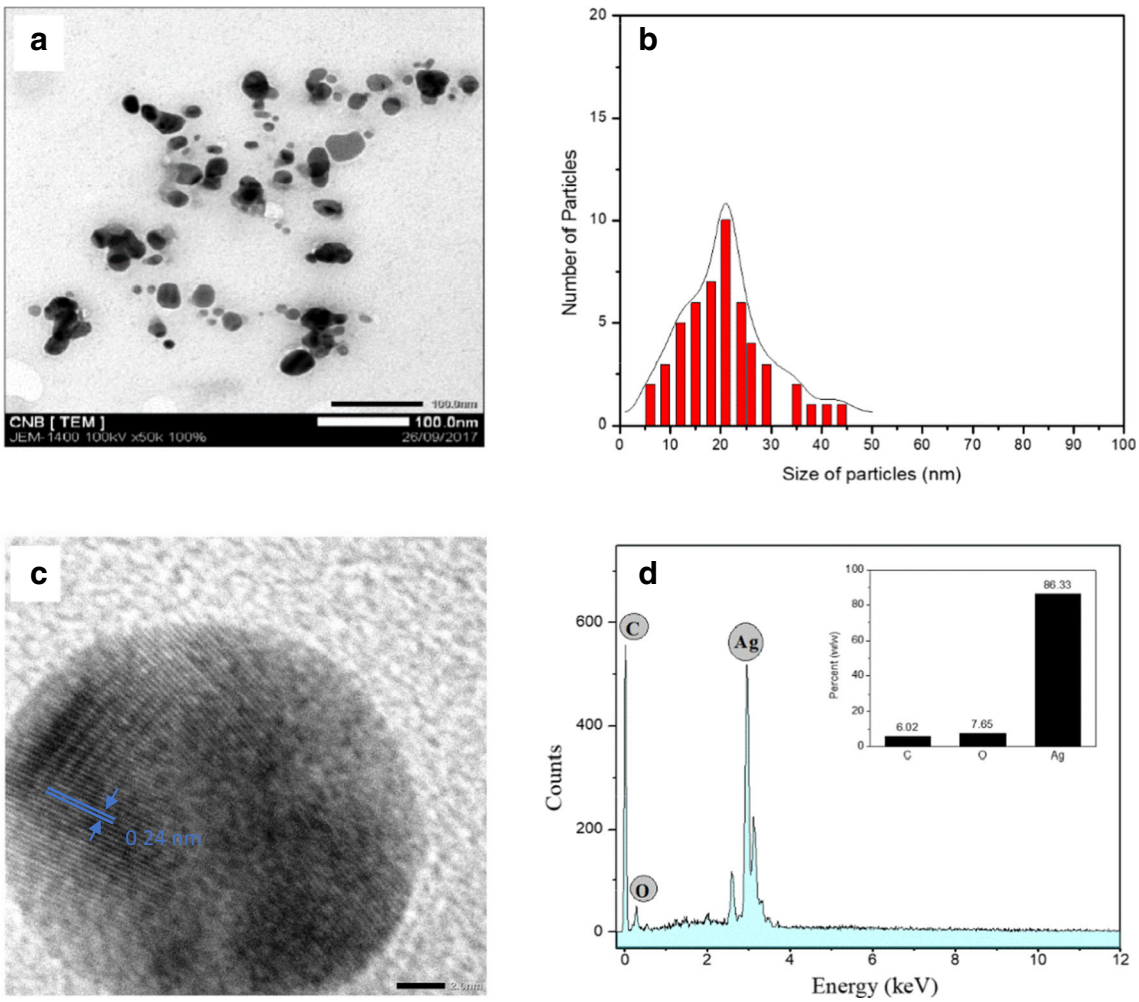

Fig. 7 TEM (a), particle size distribution (b), HRTEM (c), and EDX (d) spectrum and average content of elements (inset)

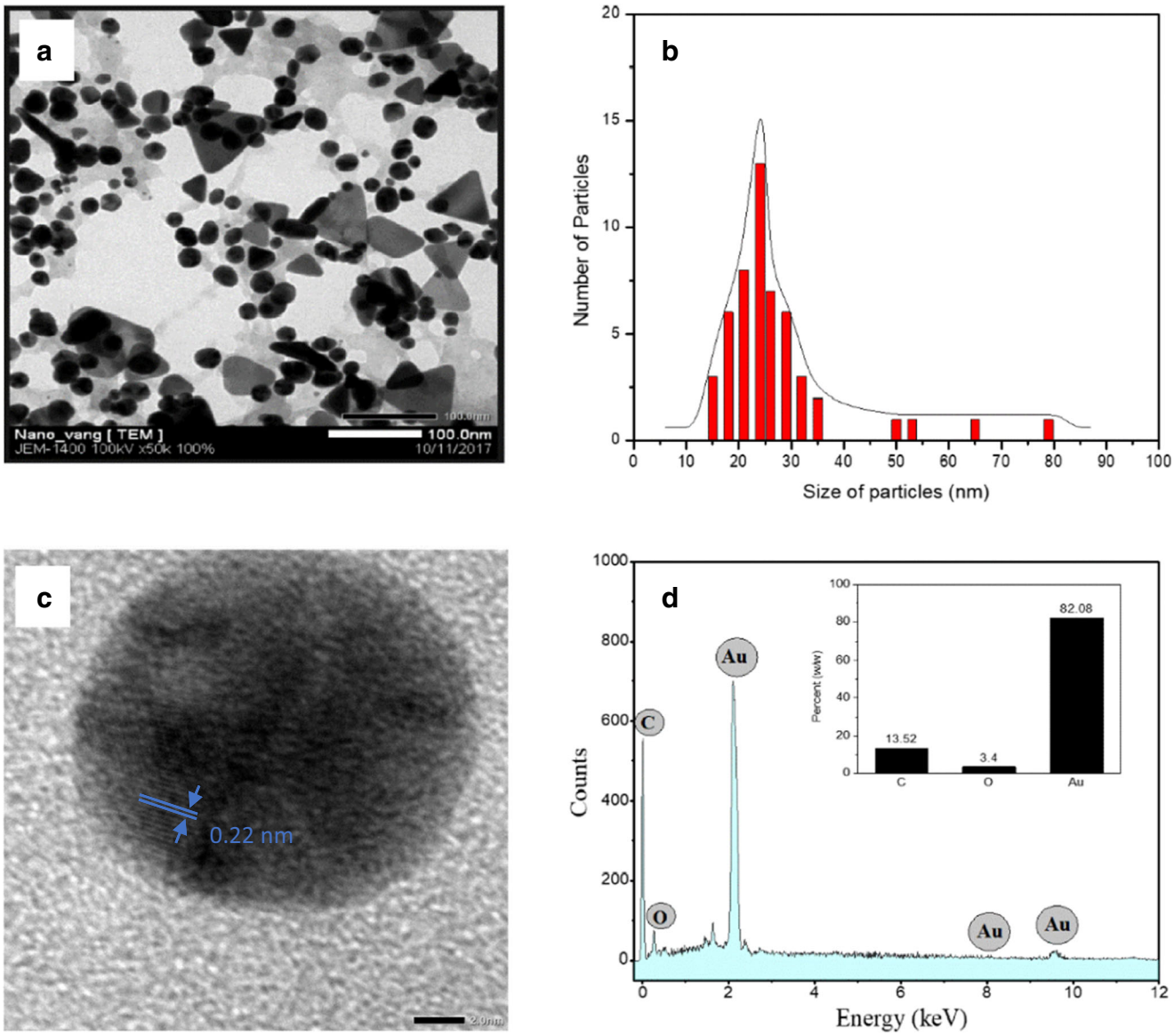

Fig. 8 TEM (a), particle size distribution (b), HRTEM (c), and EDX (d) spectrum and average content of elements (inset)

800 °C. All of the samples showed that weight loss did not occur at temperature below 100 °C (Fig. 9). It reflected that there is no moisture in the samples. Thermal decomposition of the BR extract occurs almost completely within two stages between 100 °C and 590 °C accounted for 96.1% of the total weight. On the other hand, TG curves showed that thermal properties from both MNPs biosynthesized with BR extract are similar and their thermal stability (210 °C) is significantly higher than that of BR extract (100 °C). The weight loss of BR-AgNPs and BR-AuNPs accounted for 6.5% and 14.2%, respectively, is probably due to the decomposition of BR extract on the surface of the MNPs. This observation is in agreement with average amount of MNPs in the related samples estimated from the EDX data.

DTA curve of BR extract showed that exothermic reactions occur at maximum peak of 475 °C, attributed to oxidation of organic compounds. Similar DTA results of both the biosynthesized MNPs were found. Exothermic peaks of BR-AgNPs and BR-AuNPs were observed around 370 °C. The thermal behavior of the samples shows that the BR extracts are responsible for the stabilization of MNPs.

Antimicrobial assay

The in vitro antimicrobial activity of BR-AgNPs and BR-AuNPs against five microorganisms including *E. coli* and *A. tumefaciens*, (Gram-negative); *L. acidophilus* and *S. aureus* (Gram-positive) and *T. harzianum* (fungus) was carried out. The bioactivity of both the biosynthesized MNPs is tested at the various weights. The results showed that BR-AuNPs did not inhibit any microorganisms at the tested concentrations whereas the BR-AgNPs exhibited strong activity on all the

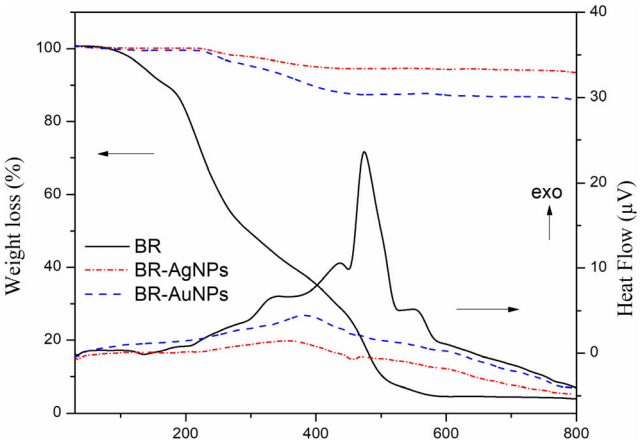

Fig. 9 Simultaneous TG and DTA curves of BR, BR-AgNPs, and BR-AuNPs in air flow of 20 mL/min at a heating rate of 10 °C/min

tested strains. The antimicrobial effect of the BR-AgNPs was plotted as growth inhibition (%) at varied concentration of the nanoparticles solution in Fig. 10. It is observed that the zones of microbial inhibition grow when increasing the concentration of AgNPs. The BR-AgNPs possess the highest antibacterial activity against *L. acidophilus* and *S. aureus*. Difference of inhibition zone of the microbials can be due to difference of their cell walls that contained the peptidoglycan layers (Saratale et al. 2018).

Catalytic performance of nanoparticles

Degradation of 4-nitrophenol

The degradation reaction of the pollutants can be carried out with $NaBH_4$ in the presence of MNPs as a catalyst, and

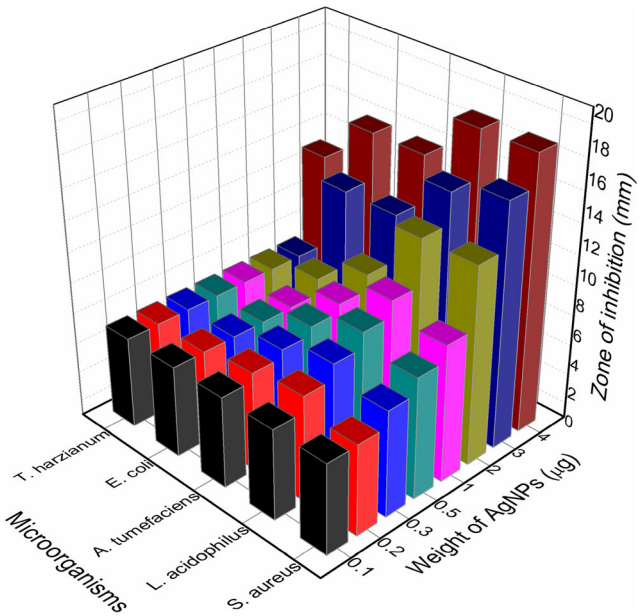

Fig. 10 Plot zone of inhibition (%) of the varied concentrations of BR-AgNPs for different microorganisms

investigating its kinetics can provide important evaluation for the reaction. The tread of catalytic potential is analyzed by scrutinizing the values of the rate constants. The rate of the degradation reactions should depend on the concentration of reactants and the catalyst. However, in the present work, the concentration of $NaBH_4$ used was very high while the concentration of the MNPs was much lower than that of the pollutants. Thus, the reaction rate is expected to be independent of both $NaBH_4$ and the catalyst, and the degradation of the pollutants should be considered as pseudo-first-order reaction with respect to the concentration of the pollutants (Corbett 1972). The reaction kinetic can be represented using the equation $\ln(A_t / A_0) = -kt$, where k is pseudo-first-order rate constant, t is the reaction time, $[A_0]$ is the concentration of 4-NP at time $t = 0$, and $[A_t]$ is the concentration at time "t" which can be obtained from the absorbance of the peak at 400 nm. The constant k can be determined directly from the slope of straight line yielded by plots of $\ln(A_t/A_0)$ versus reaction time.

4-NP has been well known as a priority pollutant by US Environmental Protection Agency (Lai et al. 2011; Ai and Jiang 2013). Due to high stability in the environment and resistant biodegradation, degradation of 4-NP is very desirable. After the addition of $NaBH_4$ to pale yellow 4-NP solution, the color of the solution changed to intense yellow and the absorption maximum peak at 317 nm was red shifted to 400 nm due to formation of 4-nitrophenolate ion in alkaline medium although no reduction occurred. As soon as the addition of BR-AgNPs and BR-AuNPs into the solution, the color of the solution is gradually disappeared. The UV-vis spectra showed the changes in absorbance of the peaks during the reaction process (Fig. 11a, c). The progressive decrease of absorbance at 400 nm and simultaneous increase of new peak at 298 nm indicated the reduction of 4-NP to form 4-aminophenol (4-AP). The results showed that the degradation of 4-NP in the presence of both the nanoparticles was completed in 12 min with evidence from almost zero absorption at 400 nm. The linear relationship can be observed from plots of $\ln(A_t/A_0)$ versus reaction time, confirmed the pseudo-first-order reactions (Fig. 11b, d). The k value in the presence of BR-AuNPs (6.87×10^{-3} s^{-1}) was slightly greater than the k value of catalyst BR-AgNPs (6.77×10^{-3} s^{-1}). In order to illustrate the catalytic advantage of the MNPs in comparison with other previous reports, some results of the 4-NP reduction have been summarized in Table 1. The results of this work show that the BR-AgNPs and BR-AuNPs reveal better catalytic performance than the other biogenic MNPs systems.

Degradation of methyl orange

Methyl orange (MO), an organic azo dye used commonly as an indicator, is one of the pollutants that generates several environmental and health problems. Thus, its degradation and removal are very interested. The catalytic degradation of

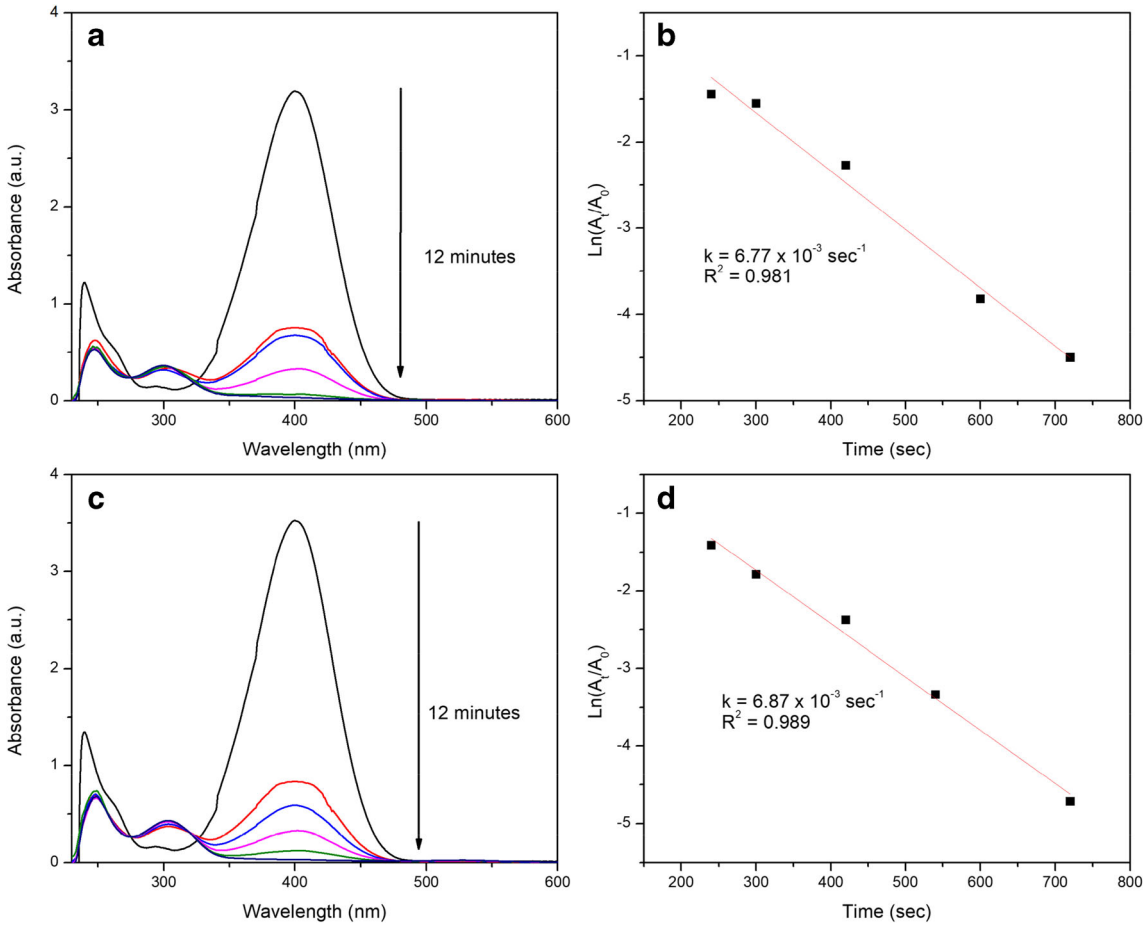

Fig. 11 UV-Vis spectra of 4-nitrophenol degradation by $NaBH_4$ in the presence of BR-AgNPs (**a**) and BR-AuNPs (**c**); first-order kinetics plotted for BR-AgNPs (**b**) and BR-AuNPs (**d**)

wastewater containing MO using MNPs as a catalyst has investigated in the literatures (Joseph and Mathew 2015b; Umamaheswari et al. 2018). The previous reports showed that the catalytic activity of MNPs for degradation of dyes depends on various conditions such as side, shape of MNPs, reductants, and stabilizers. The aqueous solution of MO is orange red color, and the UV-vis absorption spectrum of MO exhibits maxima absorption at 464 nm.

The degradation reaction of MO can be kinetically followed by the reduction of absorbance at the maxima peak with increasing time. UV-vis spectra and plot of $\ln(A_t/A_0)$ versus reaction time are presented in Fig. 12. The reduction of MO

Table 1 Comparison of the rate constants of different biogenetic AgNPs and AuNPs towards the catalytic reduction of 4-nitrophenol

MNPs	Biological system	Size (nm)	k per 1 mg of catalyst (sec^{-1})	References
AgNPs	*Ziziphus jujuba* leaf extract	20–30	2.26×10^{-3}	Gavade et al. (2015)
	Cassia occidentalis leaf extract	5–25	1.00×10^{-3}	Gondwal and Pant (2018)
	Coleus forskohlii root extract	30–40	6.70×10^{-3}	Naraginti and Sivakumar (2014)
	Arctium lappa extract	21.3	6.77×10^{-2}	This work
AuNPs	*Magnusiomyces ingens* LH-F1	28.3	1.54×10^{-3}	Qu et al. (2018)
	Artemisia dracunculus extract	100–145	3.40×10^{-3}	Wacławek et al. (2018)
	Platycodon grandiflorum	14.9	3.94×10^{-3}	Choi et al. (2018)
	Arctium lappa extract	24.7	6.87×10^{-3}	This work

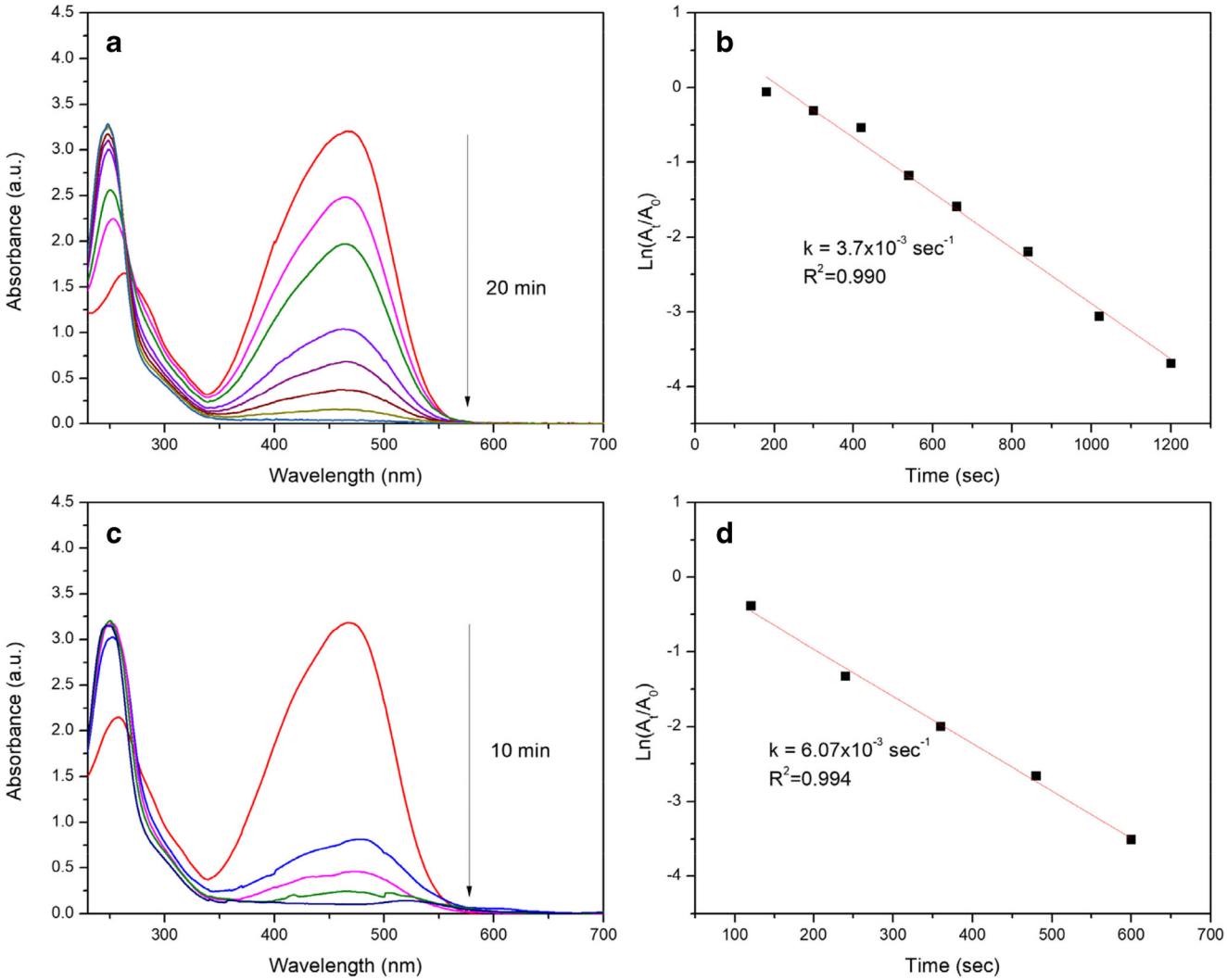

Fig. 12 UV-Vis spectra of methyl orange degradation by $NaBH_4$ in the presence of BR-AgNPs (**a**) and BR-AuNPs (**c**); first-order kinetics plotted for BR-AgNPs (**b**) and BR-AuNPs (**d**)

started immediately after the addition of the catalyst. It is evident that the decrease of absorbance at 464 nm and increase at 250 nm were observed, indicated effective catalytic degradation of MO in the presence of MNPs to form new compounds bearing NH_2 groups (Joseph and Mathew 2015b). The UV-vis spectra showed that the reaction in the presence of BR-AuNPs (10 min) was faster than that of BR-AgNPs (20 min). Moreover, the rate constant k found for catalyst BR-AuNPs (6.09×10^{-3} s^{-1}) was nearly double in comparison with that of catalyst BR-AgNPs (3.7×10^{-3} s^{-1}).

Degradation of rhodamine B

Rhodamine B (RhB), a common dye, is widely used in textile industries for various purposes and forms an important dye pollutant. The catalytic role of the BR-AgNPs and BR-AuNPs in detoxification of RhB is also determined by UV-vis absorption data as shown in Fig. 13. The catalytic degradation of RhB in the presence of the MNPs is observed by decreased intensity of the color from pink red to colorless and the reduction in intensity of the peak at 554 nm in the UV-vis spectra. The results showed that the reduction of RhB is completed within 12 min for BR-AgNPs and 10 min for BR-AuNPs. Rate constants for BR-AgNPs and BR-AuNPs for the degradation reactions are 6.07×10^{-3} s^{-1} and 7.07×10^{-3} s^{-1}, respectively.

The kinetic studies showed that the catalytic performance of BR-AuNPs is higher than that of BR-AgNPs for the degradation reaction of the used dyes. The mechanism of pollutant degradation to nontoxic and smaller molecules by $NaBH_4$ in the catalytic presence of AgNPs and AuNPs involves an electron transfer process. In this mechanism, BH_4^- ions play role as a nucleophilic source and dyes are electrophilic in nature. After the adsorption of both BH_4^- ions and dyes on the MNPs surface, the

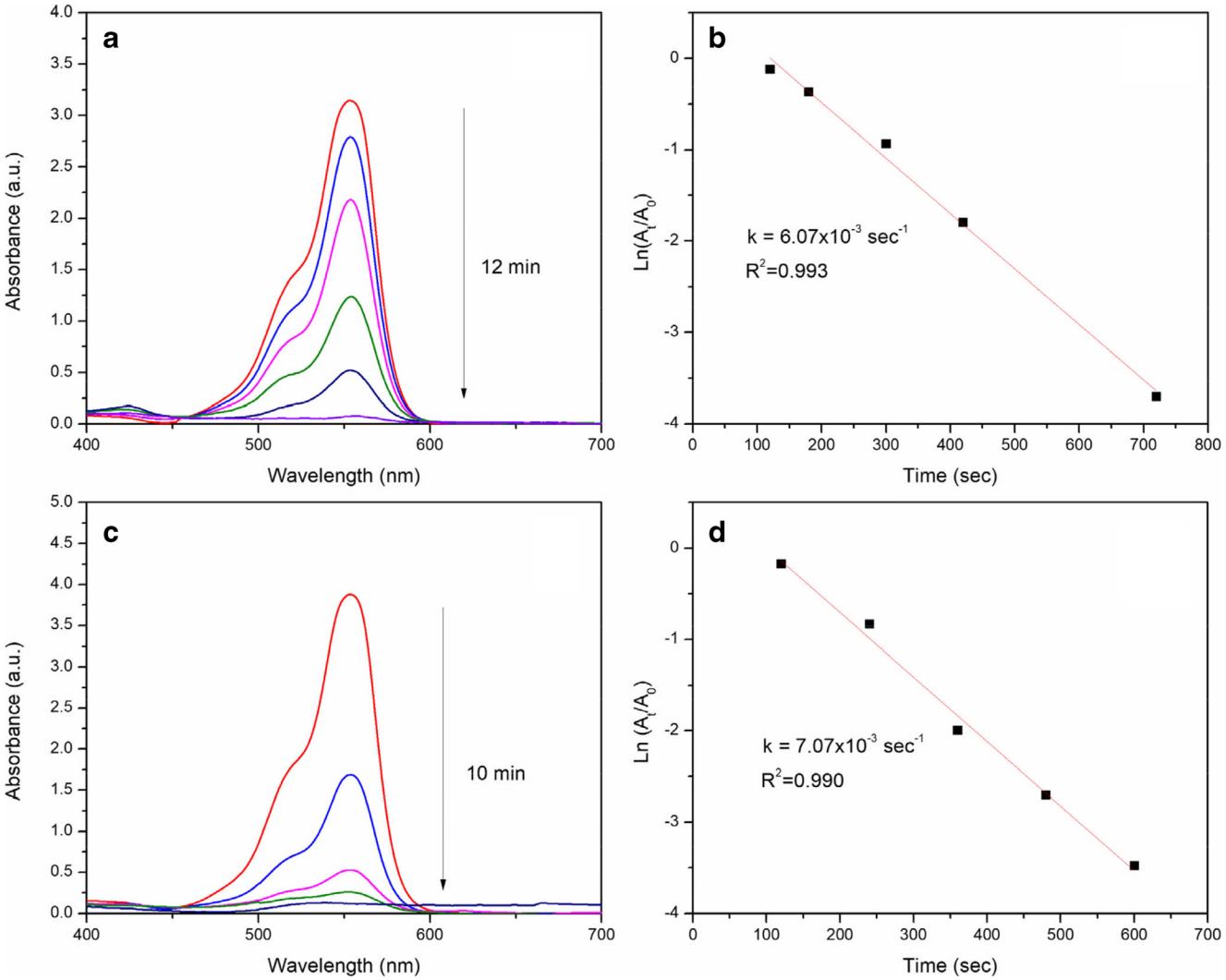

Fig. 13 UV-Vis spectra of rhodamine B degradation by $NaBH_4$ in the presence of BR-AgNPs (**a**) and BR-AuNPs (**c**), first-order kinetics plotted for BR-AgNPs (**b**) and BR-AuNPs (**d**)

MNPs transfer electrons from the donor BH_4^- ions to the acceptor dye molecules (Joseph and Mathew 2015b).

Conclusions

This study presents a simple and effective eco-friendly method alternative to common physical and chemical method for the production of MNPs using aqueous extract of *A. lappa* as the reducing and stabilizing source. Biosynthesis of AgNPs and AuNPs has been optimized based on the change of SPR absorption bands of MNPs. The nanoparticles were characterized using UV-vis, FTIR, XRD, EDX, TEM, HRTEM, and TG-DTA analyses. The BR-AgNPs and BR-AuNPs exhibited high crystallinity with an average diameter of 21.3 nm and 24.7 nm, respectively. The EDX data showed average contents of silver in BR-AgNPs and gold in BR-AuNPs being 86.3% (*w*/*w*) and 83.1% (*w*/*w*), respectively which were confirmed by TG analysis. The BR-AgNPs exhibited a high inhibition of five tested microorganism strains. The catalytic ability of the nanoparticles was investigated for the degradation of 4-nitrophenol, methyl orange, and rhodamine B by $NaBH_4$ in water medium. The reactions were very fast, and the value of the pseudo-first-order rate constants was found in the range from 3.70×10^{-3} s^{-1} to 7.08×10^{-3} s^{-1}. Therefore, this study unfolds a great possibility of biosynthesized NMPs to be applied as antimicrobial agents and green catalysts to clean the pollutants from various industrial effluents.

Funding information This project was funded by Vietnam Academy of Science and Technology (VAST) (No. ĐLTE00.04/18-19).

Compliance with ethical standards

Conflict of interest The authors declare that they have no conflict of interest.

References

Ahmed S, Ahmad M, Saifullah SBL, Ikram S (2016) Green synthesis of silver nanoparticles using Azadirachta indica aqueous leaf extract. J Radiat Res Appl Sci 9:1–7. https://doi.org/10.1016/j.jrras.2015.06.006

Ai L, Jiang J (2013) Catalytic reduction of 4-nitrophenol by silver nanoparticles stabilized on environmentally benign macroscopic biopolymer hydrogel. Bioresour Technol 132:374–377. https://doi.org/10.1016/j.biortech.2012.10.161

Albanese A, Tang PS, Chan WC (2012) The effect of nanoparticles size, shape, and surface chemistry on biological systems. Annu Rev Biomed Eng 14:1–16. https://doi.org/10.1146/annurev-bioeng-071811-150124

Arya G, Kumari RM, Gupta N, Kumar A, Channdra R, Nimesh S (2017) Green synthesis of silver nanoparticles using Prosopis juliflora bark extract: reaction optimization, antimicrobial and catalytic activities. Artif Cells Nanomed Biotechnol 18:1–9. https://doi.org/10.1080/21691401.2017.1354302

Balouiri M, Sadiki M, Ibnsouda SK (2016) Methods for in vitro evaluating antimicrobial activity: a review. J Pharm Anal 6:71–79. https://doi.org/10.1016/j.jpha.2015.11.005

Bello BA, Bello A, Khan SA, Khan JA, Syed FQ, Anwar Y, Khan SB (2017) Antiproliferation and antibacterial effect of biosynthesized AgNPs from leaves extract of Guiera senegalensis and its catalytic reduction on some persistent organic pollutants. J Photochem Photobiol B 175:99–108. https://doi.org/10.1016/j.jphotobiol.2017.07.031

Chan YS, Cheng LN, Wu JH, Chan E, Kwan YW, Lee SMY, Leung GPH, Yu PHF, Chan SW (2011) A review of the pharmacological effects of *Arctium lappa* (burdock). Inflammopharmacol 19:245–254. https://doi.org/10.1007/s10787-010-0062-4

Choi Y, Kang S, Cha SH, Kim HS, Song K, Lee YJ, Kim K, Kim YS, Cho S, Park Y (2018) Platycodon saponins from Platycodi radix (Platycodon grandiflorum) for the green synthesis of gold and silver nanoparticles, Nanoscale Res Lett (2018) 13:23 https://doi.org/10.1186/s11671-018-2436-2

Corbett JF (1972) Pseudo first-order kinetics. J Chem Educ 49:663

Dutta PP, Bordoloi M, Gogoi K, Roy S, Narzary B, Bhattacharyya DR, Mohapatra PK, Mazumder B (2017) Antimalarial silver and gold nanoparticles: green synthesis, characterization and *in vitro* study. Biomed Pharmacother 91:567–580. https://doi.org/10.1016/j.biopha.2017.04.032

Fayaz AM, Balaji K, Girilal M, Yadav R, Kalaichelvan PT, Venketesan R (2010) Biogenic synthesis of silver nanoparticles and their synergistic effect with antibiotics: a study against gram-positive and gram-negative bacteria. Nanomedicine 6:103–109. https://doi.org/10.1016/j.nano.2009.04.006

Francis S, Joseph S, Koshy EP, Mathew B (2017) Synthesis and characterization of multifunctional gold and silver nanoparticles using leaf extract of *Naregamia alata* and their applications to catalysis and control of mastitis. New J Chem 41:14288–14298. https://doi.org/10.1039/C7NJ02453C

Gavade NL, Kadam AN, Suwarnkar MB, Ghodake VP, Garadkar KM (2015) Biogenic synthesis of multi-applicative silver nanoparticles by using Ziziphus jujuba leaf extract. Spectrochim Acta A Mol Biomol Spectrosc 136:953–960. https://doi.org/10.1016/j.saa.2014.09.118

Gondwal M, Pant GJN (2018) Synthesis and catalytic and biological activities of silver and copper nanoparticles using *Cassia occidentalis*. Int J Biomater Article ID 6735426. https://doi.org/10.1155/2018/6735426

Hadacek F, Greger H (2000) Testing of antifungal natural products: methodologies, comparability of results and assay choice. Phytochem Anal 11:137–147. https://doi.org/10.1002/(SICI)1099-1565(200005/06)11:3<137::AID-PCA514>3.0.CO;2-I

Hernandez-Pinero JL, Terron-Rebolledo M, Foroughbakhch R, Moreno-Limón S, Melendrez MF, Solís-Pomar F, Pérez-Tijerina E (2016) Effect of heating rate and plant species on the size and uniformity of silver nanoparticles synthesized using aromatic plant extracts. Appl Nanosci 6:1183–1190. https://doi.org/10.1007/s13204-016-0532-0

Iravani S (2011) Green synthesis of metal nanoparticles using plants. Green Chem 13:2638–2650. https://doi.org/10.1039/C1GC15386B

Joseph S, Mathew B (2015a) Microwave assisted facile green synthesis of silver and gold nanocatalysts using the leaf extract of *Aerva lanata*. Spectrochim Acta A Mol Biomol Spectrosc 136:1371–1379. https://doi.org/10.1016/j.saa.2014.10.023

Joseph S, Mathew B (2015b) Facile synthesis of silver nanoparticles and their application in dye degradation. Mater Sci Eng B 195:90–97. https://doi.org/10.1016/j.mseb.2015.02.007

Khan T, Khan MA, Nadhman A (2015) Synthesis in plants and plant extracts of silver nanoparticles with 306 potent antimicrobial properties: current status and future prospects. Appl Microbiol Biotechnol 99:9923–9934. https://doi.org/10.1007/s00253-015-6987-1

Lai TL, Yong KF, Yu JW, Chen JH, Shu YY, Wang CB (2011) High efficiency degradation of 4-nitrophenol by microwave-enhanced catalytic method. J Hazard Mater 185:366–372. https://doi.org/10.1016/j.jhazmat.2010.09.044

Mahadevan S, Vijayakumar S, Arulmozhi P (2017) Green synthesis of nanoparticles from *Atalantia monophylla* (L) Correa leaf extract, their antimicrobial activity and sensing capability of H_2O_2. Microb Pathog 113:445–450. https://doi.org/10.1016/j.micpath.2017.11.029

Misha A, Kumari M, Pandey S, Chaudhry V, Gupta K, Nautiyal C (2014) Biocatalytic and antimicrobial activities of gold nanoparticles synthesized by *Trichoderma* sp. Bioressour technol 166:235–142. https://doi.org/10.1016/j.biortech.2014.04.085

Morales-Luckie RA, Lopezfuentes-Ruiz AA, Olea-Mejía OF, Liliana A-F, Sanchez-Mendieta V, Brostow W, Hinestroza JP (2016) Synthesis of silver nanoparticles using aqueous extracts of *Heterotheca inuloides* as reducing agent and natural fibers as templates: Agave lechuguilla and silk. Mater Sci Eng C 69:429–436. https://doi.org/10.1016/j.msec.2016.06.066

Nag S, Pramanik A, Chattopadhyay D, Bhattacharyya M (2018) Green-fabrication of gold nanomaterials using *Staphylococcus warneri* from Sundarbans estuary: an effective recyclable nanocatalyst for degrading nitro aromatic pollutants. Environ Sci Pollut Res 25:2331–2349. https://doi.org/10.1007/s11356-017-0617-7

Naraginti S, Li Y (2017) Preliminary investigation of catalytic, antioxidant, anticancer and bactericidal activity of green synthesized silver and gold nanoparticles using Actinidia deliciosa. J Photochem Photobiol B 170:225–234. https://doi.org/10.1016/j.jphotobiol.2017.03.023

Naraginti S, Sivakumar A (2014) Eco-friendly synthesis of silver and gold nanoparticles with enhanced bactericidal activity and study of silver catalyzed reduction of 4-nitrophenol. Spectrochim Acta A Mol Biomol Spectrosc 128:357–362. https://doi.org/10.1016/10.1016/j.saa.2014.02.083

Nguyen TD, Dang VS, Nguyen VH, Nguyen TMT, Dang CH (2018a) Synthesis and photophysical characterization of several 2,3-quinoxaline derivatives. An application of Pd(0)/PEG nanoparticle catalyst for Sonogashira coupling. Polycycl Aromat Compd 38:42–50. https://doi.org/10.1080/10406638.2016.1143848

Nguyen TD, Dang CH, Mai DT (2018b) Biosynthesized AgNP capped on novel nanocomposite 2-hydroxypropyl-β-cyclodextrin/alginate as a catalyst for degradation of pollutants. Carbohyd Polym 197:29–37. https://doi.org/10.1016/j.carbpol.2018.05.077

Prakash P, Gnanaprakasam P, Emmanuel R, Arokiyaraj S, Saravanan M (2013) Green synthesis of silver nanoparticles from leaf extract of *Mimusops elengi*, Linn. for enhanced antibacterial activity against

multi drug resistant clinical isolates. Colloids Surf B Biointerfaces 108:255–259. https://doi.org/10.1016/j.colsurfb.2013.03.017

Pramanik N, Bhattacharyya A, Kundu PP (2015) Spectroscopic analysis and catalytic application of biopolymer capped silver nanoparticles, an effective antimicrobial agent. J Appl Polym Sci 132(41495). https://doi.org/10.1002/app.41495

Qu Y, You S, Zhang X, Pei X, Shen W, Li Z, Li S, Zhang Z (2018) Biosynthesis of gold nanoparticles using cell-free extracts of *Magnusiomyces ingens* LH-F1 for nitrophenols reduction. Bioprocess Biosyst Eng 41(3):359–367. https://doi.org/10.1007/s00449-017-1869-9

Rafique M, Sadaf I, Rafique MS, Tahir MB (2017) A review on green synthesis of silver nanoparticles and their applications. Artif Cells Nanomed Biotechnol 45:1272–1291. https://doi.org/10.1080/21691401.2016.1241792

Saratale RG, Shin HS, Kumar G, Benelli G, Ghodake GS, Jiang YY, Kim DS, Saratale GD (2018) Exploiting fruit byproducts for eco-friendly nanosynthesis: Citrus × clementina peel extract mediated fabrication of silver nanoparticles with high efficacy against microbial pathogens and rat glial tumor C6 cells. Environ Sci Pollut Res 25:10250–10263. https://doi.org/10.1007/s11356-017-8724-z

Sathishkumar M, Sneha K, Won S, Cho CW, Kim S, Yun YS (2009) Cinnamon zeylanicum bark extract and powder mediated green synthesis of nano-crystalline silver particles and its bactericidal activity. Colloids Surf B Biointerfaces 73:332–338. https://doi.org/10.1016/j.colsurfb.2009.06.005

Schrofel A, Kratosova G, Safarik I, Safarikova M, Raska I, Shor LM (2014) Applications of biosynthesized metallic nanoparticles – a review. Acta Biomater 10:4023–4042. https://doi.org/10.1016/j.actbio.2014.05.022

Sheny D, Mathew J, Philip D (2011) Phytosynthesis of Au, Ag and Au–Ag bimetallic nanoparticles using aqueous extract and dried leaf of *Anacardium occidentale*. Spectrochim Acta A Mol Biomol Spectrosc 79:254–262. https://doi.org/10.1016/j.saa.2011.02.051

Singh P, Kim YJ, Zhang D, Yang DC (2016a) Biological synthesis of nanoparticles from plants and microorganisms. Trends Biotechnol 34:588–599. https://doi.org/10.1016/j.tibtech.2016.02.006

Singh P, Kim YJ, Wang C, Mathiyalagan R, Yang DC (2016b) The development of a green approach for the biosynthesis of silver and gold nanoparticles by using Panax ginseng root extract, and their biological applications. Artif Cells Nanomed Biotechnol 44:1150–1157. https://doi.org/10.3109/21691401.2015.1011809

Singh P, Kim YJ, Yang DC (2015) A strategic approach for rapid synthesis of gold and silver nanoparticles by Panax ginseng leaves. Artif Cells Nanomed Biotechnol 44:1949–1957. https://doi.org/10.3109/21691401.2015.1115410

Tareq FK, Fayzunnesa M, Kabir MS (2017) Antimicrobial activity of plant-median synthesized silver nanoparticles against food and agricultural pathogens. Microb Pathog 109:228–232. https://doi.org/10.1016/j.micpath.2017.06.002

Tousch D, Bidel LPR, Cazals G, Ferrare K, Leroy J, Faucanie M, Chevassus H, Tournier M, Lajoix AD, Azay-Milhau J (2014) Chemical analysis and antihyperglycemic activity of an original extract from burdock root (*Arctium lappa*). J Agric Food Chem 62:7738–7745. https://doi.org/10.1021/jf500926v

Umamaheswari C, Lakshmanan A, Nagarajan NS (2018) Green synthesis, characterization and catalytic degradation studies of gold nanoparticles against Congo red and methyl orange. J Photochem Photobiol B 178:33–39. https://doi.org/10.1016/j.jphotobiol.2017.10.017

Wacławek S, Gončuková Z, Adach K, Fijałkowski M, Černík M (2018) Green synthesis of gold nanoparticles using Artemisia dracunculus extract: control of the shape and size by varying synthesis conditions. Environ Sci Pollut Res Int 25(24):24210–24219 https://doi.org/10.1007/s11356-018-2510-4

Zhang S, Tang Y, Vlahovic B (2016) A review on preparation and applications of silver-containing nanofibers. Nanoscale Res Lett, 11 11:80–87. https://doi.org/10.1186/s11671-016-1286-z

Zhao L, Shen G, Ma G, Yan X (2016) Engineering and delivery of nanocolloids of hydrophobic drugs. Adv Colloid Interf Sci 249:308–320. https://doi.org/10.1016/j.cis.2017.04.008